Check for updates

Simplified LDPC-assisted CNC algorithm for entropy-loaded discrete multi-tone in a 100G flexible-rate PON

WENXUAN MO,[1] ID JI ZHOU,[1,2,*] GENGCHEN LIU,[3] YUANDA HUANG,[3] LIANGCHUAN LI,[3,5] HAN CUI,[4] HAIDE WANG,[1] QINGXIN LU,[1] WEIPING LIU,[1] AND CHANGYUAN YU[2] ID

[1]*Department of Electronic Engineering, Jinan University, Guangzhou, 510632, China*
[2]*Department of Electronic and Information Engineering, The Hong Kong Polytechnic University, Hong Kong, China*
[3]*Optical Research Department, Huawei Technologies, Dongguan, 523808, China*
[4]*State Key Laboratory of Information Photonics and Optical Communications, School of Information and Communication Engineering, Beijing University of Posts and Telecommunications, Beijing, 100876, China*
[5]*liliangchuan@huawei.com*
[*]*zhouji@jnu.edu.cn*

Abstract: Passive optical networks (PONs) have been widely used in optical access networks to meet the requirement of the rapidly growing data traffic. However, the optical power budget of the worst optical network unit certainly limits the maximum capacity of PON. In this paper, we demonstrate a flexible-rate PON based on entropy-loaded clipping discrete multi-tone (DMT) for increasing the capacity. Meanwhile, clipping operation and simplified low-density parity-check (LDPC) assisted clipping-noise-cancellation (CNC) algorithm are proposed to improve the performance of DMT in peak-power constrained PON. In the simplified LDPC-assisted CNC algorithm, the iteration number of the sum-product algorithm in the LDPC decoding can be reduced to decrease the computational complexity almost without performance loss. The experimental results show that the simplified CNC algorithm can achieve approximately 1.8dB improvement of the optical receiver sensitivity at the 20% soft-decision forward-error-correction limit. The proposed flexible-rate PON has a wide-range data-rate adjustment from 12.5Gb/s to 100Gb/s under the optical power budget from 40dB to 26dB.

1. Introduction

Intensity modulation and direct detection (IM/DD) system is widely used in short-distance optical communication scenarios such as passive optical networks (PONs) as it features the advantages of low cost, low power consumption, and high reliability [1–3]. To meet the requirement of the rapidly growing data traffic, PONs have been widely used in optical access networks [4–6]. However, the maximum data rate of PON is limited by the optical power budget of the worst optical network unit (ONU). Although the digital signal process (DSP) is employed in the 50 Gb/s PON to increase the optical power budget, it is still on the brink of a 31dB optical power budget for meeting the requirement of the whole ONUs [7–10]. Moreover, as the optical power budget of the worst ONU certainly limits the maximum capacity of PON [11–13], flexible-rate data should be delivered to match the optical power budget of each ONU to increase the capacity.

A new 100 Gb/s fine-granularity flexible-rate PON based on adaptive-bit-and-power-loaded discrete multi-tone (ABPL-DMT) is proposed to implement a fine-granularity flexible-rate adjustment of the data rate in our previous work [14]. Compared with the ABPL-DMT, the entropy-loaded DMT with probabilistic constellation shaping (PCS) technology regulates the uniform quadrature-amplitude modulation (QAM) formats to PCS-QAM with approximate

Gaussian distribution, the flexible rate adaptation can be realized by adjusting the shaping entropy of the signals, which can provide more granular and flexible-rate adjustment [15–18]. However, the DMT signal suffers from a systematic problem of a high peak-to-average power ratio (PAPR) compared to the single-carrier signal [19–21]. High PAPR results in low average power of the transmitted signal, leading to a low signal-to-noise ratio (SNR) of the received signal in peak-power constrained PON. Many PAPR reduction methods have been researched, such as partial transmit sequence, tone reservation, active constellation extension, and clipping [22–25]. Among such PAPR reduction methods, clipping is a straightforward and commonly-used method to reduce the PAPR for DMT signal [26–29]. However, clipping the peak of the DMT signal introduces the clipping noise simultaneously, which causes the degradation of system performance.

In our previous works, an effective low-density parity-check assisted clipping-noise-cancellation (LDPC-assisted CNC) algorithm is proposed to eliminate the impact of clipping noise [30–32]. In such an LDPC-assisted CNC algorithm, the sum-product algorithm (SPA) with a large iteration number is adopted in the LDPC decoder to correct the error bits for estimating an accurate clipping noise. However, the multiple iteration processes in the LDPC decoder increase the computational complexity of the CNC algorithm. In this paper, we proposed a simplified LDPC-assisted CNC algorithm for the entropy-loaded DMT system, in which the iteration number of the SPA in the LDPC decoding can be reduced to decrease the computational complexity almost without performance loss. The main contributions of this paper are:

- The simplified CNC algorithm is proposed for the entropy-loaded clipping DMT in flexible-rate PON, which can estimate and eliminate the accurate clipping noise to improve the optical power budget. A segment LDPC decoder with adaptive adjustment of iteration is proposed for reducing the computational complexity of the CNC algorithm.

- We set up an experiment of the entropy-loaded clipping DMT with the simplified CNC algorithm for flexible-rate PON. The experimental results show that the entropy-loaded clipping DMT with a simplified CNC algorithm can achieve a wide-range data-rate adjustment from 12.5Gb/s to 100Gb/s under the optical power budget from 40dB to 26dB.

The rest of this paper is organized as follows. In Section 2, the simplified CNC algorithm for eliminating the clipping noise is described in detail. In Section 3, the experimental setups and DSP are introduced. In Section 4, the experimental results are analyzed. Finally, this paper is concluded in Section 5.

2.   Simplified LDPC-assisted CNC algorithm

High PAPR is an innate problem for DMT signals. The high-PAPR DMT signal has low average power, resulting in a low optical power budget in peak-power constrained PON. To meet the requirement of a high optical power budget in PON, the symmetric-clipping operation is adopted to reduce the PAPR of entropy-loaded DMT signal, and the CNC algorithm is employed to effectively eliminate the clipping noise introduced by clipping operation [30]. To estimate and eliminate the clipping noise more accurately, the SPA with a large iteration number is adopted in the LDPC decoder to correct the error bits. However, such decoding processes increase the computational complexity of the CNC algorithm. To reduce the complexity of the CNC algorithm, we propose a simplified CNC algorithm with a segment LDPC decoder.

Figure 1(a) shows the diagram of the simplified CNC algorithm for entropy-loaded clipping DMT system. Firstly, the received time-domain clipping DMT signals are converted into PCS-QAM symbols and clipping noise by fast-Fourier transform (FFT). After that, the log-likelihood-ratio (LLR) of each recovered bit is calculated by log-maximum a posterior probability (Log-MAP) estimation and sent to the proposed segment LDPC decoder with m times iteration
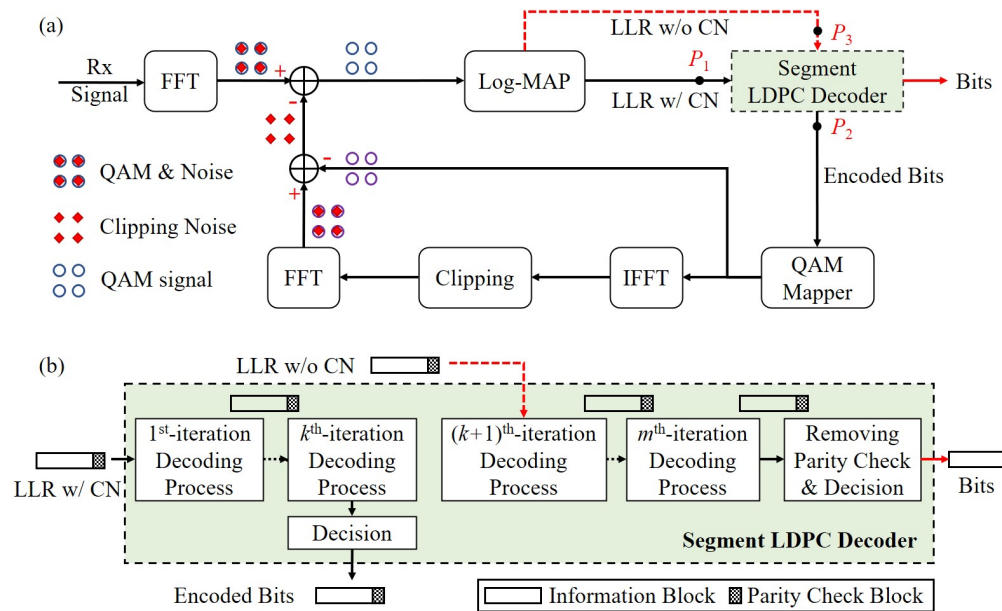
Fig. 1. (a) Diagram of the simplified CNC algorithm for entropy-loaded clipping DMT. (b) Process of the proposed segment LDPC decoder for CNC algorithm.

decoding process using the SPA [33], as shown in Fig. 1(b). As the information bits and parity check bits are updated during each iteration, these encoded bits can be sent to the QAM mapper to regenerate PCS-QAM signals after k^{th} ($k<m$) iteration decoding process. Then, the clipping DMT signals are regenerated by inverse FFT (IFFT) and clipping. After the FFT, the regenerated PCS-QAM signal with clipping noise subtracts the regenerated PCS-QAM signal without clipping noise to estimate the clipping noise. Finally, the recovered PCS-QAM symbols subtract the estimated clipping noise to extract more precise PCS-QAM symbols.

In the simplified CNC algorithm, the iteration number k influences the bit error ratio (BER) of the corrected bits. The BER of the corrected bits determines the accuracy of the estimated clipping noise. Generally, the SPA-based iteration process terminates when reaching the maximal iteration to make certain that all corrected bits c satisfy the parity-check function $cH^T = 0$, where H represents the parity-check matrix, and $(\cdot)^T$ donates the transpose operation. However, fewer bits are corrected by the LDPC decoder and the complexity increases as k increases. When 99.8% of the corrected bits satisfy the parity-check function, the regenerated clipping DMT signal is close to the original one, and the estimated clipping noise is accurate. Therefore, the iteration process can be cut off to reduce the complexity with almost no performance loss, even if the BER of the corrected bits is approximately 10^{-4}, instead of 10^{-12}.

As LDPC iteration k increases, more error bits are corrected by the iteration process, and the BER of the corrected bits before the CNC algorithm (i.e., the BER at Point P_2 in Fig. 1) decreases linearly, as shown in Fig. 2(a). $k = 0$ represents the BER before LDPC decoding (i.e., the BER at Point P_1 in Fig. 1). The BER of the corrected bits before the CNC algorithm reaches 10^{-12} with more than 20 times iteration processes, while the BER of that reaches 10^{-4} with only 6 times iteration processes. In addition, the corrected bits are used for regenerating the PCS-QAM symbols, which influence the accuracy of the estimated clipping noise. In consequence, the BER of the corrected bits before the CNC algorithm influences the pre-FEC BER after the CNC algorithm (i.e., the BER at Point P_3 in Fig. 1). As shown in Fig. 2(b), the pre-FEC BER after the CNC algorithm decreases firstly as LDPC iteration k increases and tends to be stable after 6 times
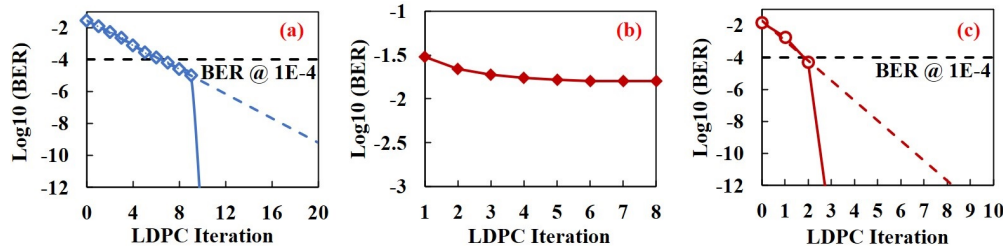
Fig. 2. (a) BER of the corrected bits before CNC algorithm versus LDPC iteration. (b) Pre-FEC BER after CNC algorithm versus LDPC iteration. (c) Post-FEC BER after CNC algorithm versus LDPC iteration. The dashed blue and red lines represent the trend line of the BER.

iteration processes. That is, the corrected bits are precise enough to estimate clipping noise, and the iteration process can be terminated after 6 times iteration processes. Obviously, by relaxing the conditions of satisfaction for LDPC decoding, the required iteration times can be reduced, which can dramatically reduce the complexity of the CNC algorithm. After removing the clipping noise by the CNC algorithm, the SNR of the PCS-QAM symbols is improved, resulting in a quick decrease of the post-FEC BER, as shown in Fig. 2(c).

Figure 3(a) shows the recovered PCS-256QAM of the entropy-loaded clipping DMT signal before the CNC algorithm. The BER of the recovered PCS-256QAM without the CNC algorithm is approximately 0.018. The estimated clipping noise by the LDPC-assisted CNC algorithm is shown in Fig. 3(b). After estimating the clipping noise by the CNC algorithm, the recovered PCS-256QAM is shown in Fig. 3(c) and the BER of the recovered PCS-256QAM in Fig. 3(c) is approximately 0.0011. Obviously, the recovered PCS-256QAM in Fig. 3(c) is more clear than that in Fig. 3(a), and the BER of entropy-loaded clipping DMT with the CNC algorithm is one-tenth of that without the CNC algorithm. In consequence, the performance of the entropy-loaded clipping DMT can be further improved when the clipping noise is effectively removed.
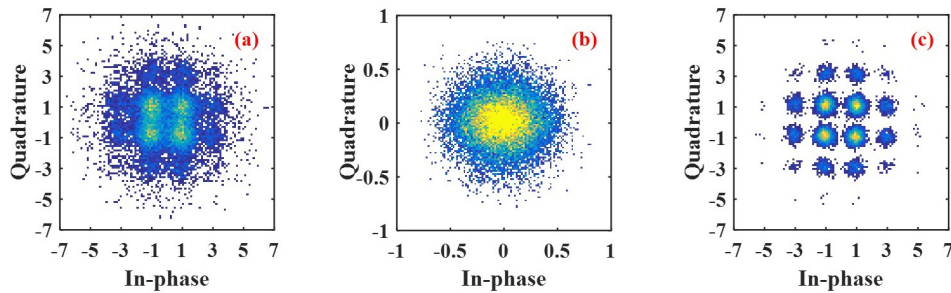

Fig. 3. (a) The recovered PCS-256QAM of entropy-loaded clipping DMT signal before CNC algorithm. (b) The estimated clipping noise. (c) The recovered PCS-256QAM of entropy-loaded clipping DMT signal after CNC algorithm for 50Gb/s ONUs.

3. Experimental setups

We set up an experiment of entropy-loaded clipping DMT for flexible-rate PON to certify the benefit of the simplified CNC algorithm and the flexible adjustment of data rate. Figure 4(a) shows the experimental setups of entropy-loaded clipping DMT. At the transmitter end, the entropy-loaded clipping DMT signal is generated by the DSP of the transmitter (Tx). The line rate of the generated entropy-loaded DMT signal (i.e., R_4 in Fig. 4(b)) is equal to $(R_2 + R_3)/r$,
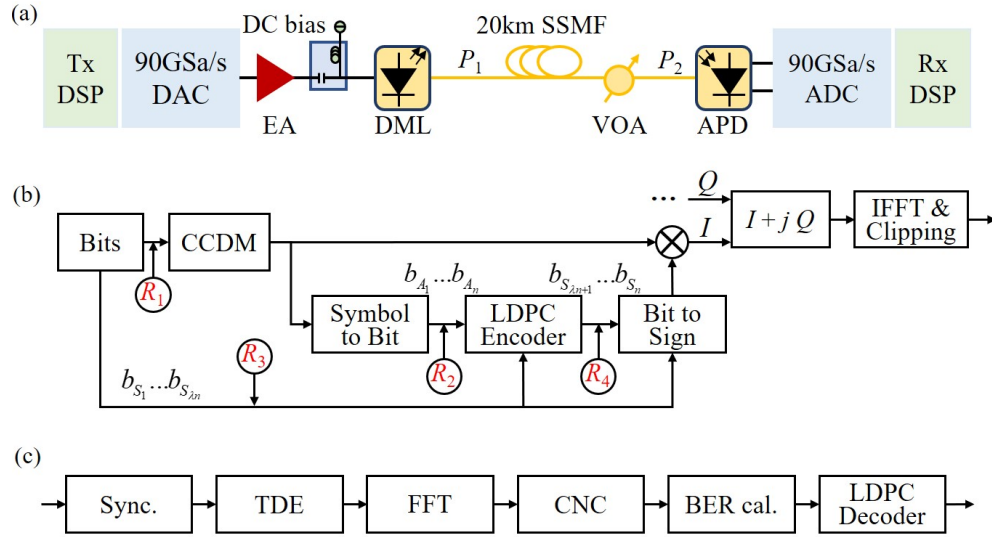
Fig. 4. (a) Experimental setups of entropy-loaded clipping DMT. (b) Tx DSP and (c) Rx DSP for entropy-loaded clipping DMT.

where r represents the LDPC code rate. For the flexible-rate PON transmission scenario, the effective line rate only includes payload in PCS and FEC overhead for payload in PCS, which is equal to $(R_1 + R_3)/r$. In the following sections of this paper, the data rate denotes the effective line rate if there is no special statement.

The entropy-loaded clipping DMT signal is converted into an analog signal by a 90GSa/s digital-to-analog converter (DAC) with a 3dB bandwidth of 16GHz. An electrical amplifier (EA, CENTELLAX OA4SMM4) is used for amplifying the analog signal. After that, the amplified analog signal is modulated on a 1304nm optical carrier by a 10G directly modulated laser (DML, NEL NLK 1352UGH). The optical signal is then launched into 20km standard single-mode fiber (SSMF) with the launch optical power of 9.78dBm, which can be measured at P_1 in Fig. 4(a). At the receiver end, a variable optical attenuator (VOA) is used to adjust the received optical power (ROP). The ROP can be measured at P_2 in Fig. 4(a). The optical power budget can be calculated by the difference in optical power between P_1 and P_2. A 25GHz avalanche photo-diode (APD) is used for converting the optical signal to an electrical signal. The electrical signal is then sent to a 90GSa/s analog-to-digital converter (ADC) to convert to a digital signal. Finally, the DSP of the receiver (Rx) is used for recovering the transmitted signal from the received digital signal.

Figures 4(b) and (c) show the Tx and Rx DSP of entropy-loaded clipping DMT. We use probabilistic amplitude shaping (PAS) to acquire PCS-QAM symbols [34]. Firstly, the bit sequence is sent to constant composition distribution matching (CCDM) to transform the uniformly distributed bits into amplitudes with the desired distribution. The n amplitudes output $A_1 \ldots A_n$ from CCDM is transformed into amplitude bits. These amplitude bits and another λn data bits are then sent to the LDPC encoder with 20% overhead to obtain $(1 - \lambda)n$ check bits. The code length of the employed LDPC is 8448, and the code rate is set to 0.833. These check bits and the λn data bits are transformed into signs $S_1 \ldots S_n$. The $b_{A_1} \ldots b_{A_n}$ and the $b_{S_1} \ldots b_{S_n}$ in Fig. 4(b) are amplitude and sign bits respectively. After that, the amplitude shift keying (ASK) symbols X_i are generated by $S_i \cdot A_i$, where $i = 1 \ldots n$. Then two ASK symbols are mapped to the in-phase and quadrature components of the PCS-QAM symbols. As the maximum entropy for the flexible-rate PON is larger than 6 bits/symbol, the PCS-256QAM symbols are generated during the experiment. The PCS-256QAM symbols are then fed into 1024-point IFFT to generate
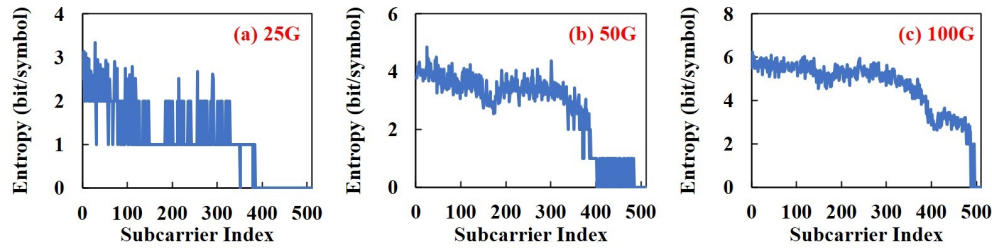
Fig. 5. Entropy for (a) 25Gb/s, (b) 50Gb/s, and (c) 100Gb/s ONUs, respectively.

the entropy-loaded DMT signals. Finally, the peaks of the entropy-loaded DMT signals are clipped to reduce the PAPR. The PAPR of the clipped DMT signal is 6.48 dB. At the receiver end, the Rx DSP is mainly comprised of a time-domain equalizer (TDE) used for compensating the distortions caused by the channel, and the CNC algorithm for removing the clipping noise.

4. Results and discussion

Figures 5(a)-(c) show the entropy of each subcarrier for ONUs with the data rate of 25Gb/s, 50Gb/s, and 100Gb/s, respectively. For 25Gb/s ONUs, the entropy of most subcarriers is 1 bit/symbol or 2 bits/symbol, and the maximum entropy is about 3.3 bits/symbol. For 50Gb/s ONUs, the entropy of most subcarriers is larger than 2 bit/symbol, which is in the interval between 2 bits/symbol and 5 bits/symbol. The maximum entropy for 50Gb/s ONUs is about 4.8 bits/symbol. For 100Gb/s ONU, the entropy of most subcarriers is in the interval between 2 bits/symbol and 6 bits/symbol, while only a few subcarriers with entropy is less than 2 bits/symbol. The maximum entropy for 100Gb/s ONUs is about 6.2 bits/symbol.

Figures 6(a)-(c) show the BER performance versus ROP for the ONUs with the rate of 25Gb/s, 50Gb/s, and 100Gb/s in the flexible-rate entropy-loaded DMT with and without CNC algorithm, respectively. For 25Gb/s ONUs, when the ROP is higher than −29dBm, the BER of the entropy-loaded clipping DMT with CNC algorithm is lower than 20% soft-decision forward-error-correct (SD-FEC) limit of 0.024, and the receiver sensitivity of the entropy-loaded clipping DMT with CNC algorithm is 1.8dB higher than that without CNC algorithm. For 50Gb/s ONUs, when the ROP is higher than −25dBm, the BER of the entropy-loaded clipping DMT with CNC algorithm is lower than 20% SD-FEC limit, and the receiver sensitivity of the entropy-loaded clipping DMT with CNC algorithm is 1.8dB higher than that without CNC algorithm. For 100Gb/s ONUs, when the ROP is higher or equal to −16dBm, the BER of the entropy-loaded clipping DMT with the CNC algorithm is lower than 20% SD-FEC limit, while the entropy-loaded clipping DMT without CNC algorithm can not reach the same 20% SD-FEC limit even when ROP is −15dBm. Figures 7(a)-(c) show the BER performance comparison of signals between the simplified and traditional CNC for 25Gb/s, 50Gb/s and (c) 100Gb/s ONUs. Comparing with the traditional CNC algorithm, there is almost no performance loss using the simplified CNC algorithm.

Figures 8(a) and (b) show the data rate and spectral efficiency versus the optical power budget at the 20% SD-FEC limit for the ONUs in the flexible-rate entropy-loaded DMT with and without CNC algorithm. The data rate can be adjusted from 100Gb/s to 12.5Gb/s under the optical power budget from 26dB to 40dB. The spectral efficiency can also be adjusted from 2bit/s/Hz to 0.25bit/s/Hz with the optical power budget from 26dB to 40dB. The optical power budget for the 100Gb/s ONUs is 26dB, and the optical power budget for the 12.5Gb/s ONUs is 40dB, which supports ONUs with the minimum and maximum optical path losses. Therefore, the experimental results certify the benefit of the simplified CNC algorithm and the flexible adjustment of data rate for the 100G flexible-rate PON is feasible.
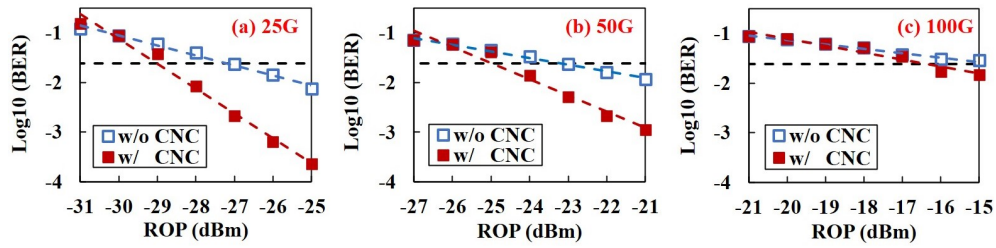
Fig. 6. The BER performance versus ROP for the ONUs with the rate of (a) 25Gb/s, (b) 50Gb/s, and (c) 100Gb/s in the flexible-rate entropy-loaded DMT, respectively. The dashed black lines represent the 20% SD-FEC limit.
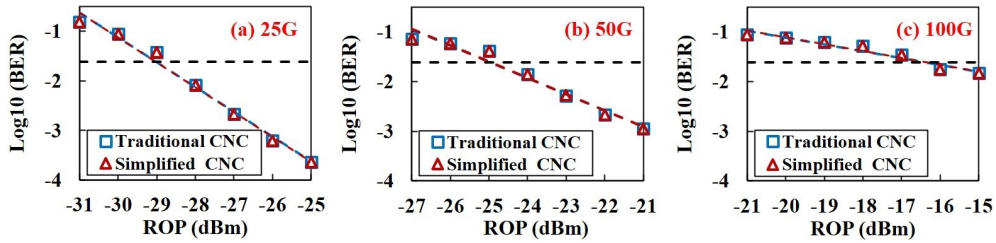

Fig. 7. The BER performance comparison of signals between the simplified and traditional CNC for (a) 25Gb/s, (b) 50Gb/s and (c) 100Gb/s ONUs. The dashed black lines represent the 20% SD-FEC limit.
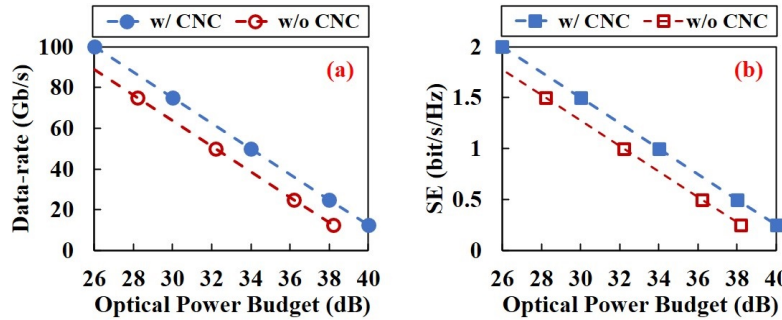

Fig. 8. (a) Data rate and (b) spectral efficiency versus optical power budget at the 20% SD-FEC limit for the ONUs in the flexible-rate entropy-loaded DMT with and without CNC algorithm.

5. Conclusion

In this paper, we proposed a flexible-rate PON based on entropy-loaded clipping DMT for increasing capacity. Meanwhile, clipping operation and simplified LDPC-assisted CNC algorithm are proposed to improve the performance of DMT. To reduce the computational complexity of the CNC algorithm, a segment LDPC decoder is proposed for reducing the iteration number in the decoding process. The experimental results show that the entropy-loaded DMT with the simplified CNC algorithm in the 100G flexible-rate PON for 25Gb/s and 50Gb/s ONUs achieve about 1.8dB higher receiver sensitivity compared to that without the CNC algorithm. For 100Gb/s ONUs, the BER of the entropy-loaded clipping DMT with the CNC algorithm is lower than 20% SD-FEC limit when the ROP is higher or equal to −16dBm, while the BER of that without the CNC algorithm cannot reach the same limit. In conclusion, the proposed flexible-rate

PON has a wide-range data-rate adjustment from 12.5Gb/s to 100Gb/s under the optical power budget from 40dB to 26dB.

Disclosures. The authors declare no conflicts of interest.

Data availability. Data underlying the results presented in this paper are not publicly available at this time but may be obtained from the authors upon reasonable request.

References

1. X. Pang, O. Ozolins, L. Zhang, A. Udalcovs, R. Lin, R. Schatz, U. Westergren, S. Xiao, W. Hu, G. Jacobsen, S. Popov, and J. Chen, "Beyond 200 Gbps per lane intensity modulation direct detection (IM/DD) transmissions for optical interconnects: Challenges and recent developments," in *Optical Fiber Communication Conference*, (Optical Society of America, 2019), pp. W4I–7.
2. D.-Z. Hsu, C.-C. Wei, H.-Y. Chen, W.-Y. Li, and J. Chen, "Cost-effective 33-Gbps intensity modulation direct detection multi-band OFDM LR-PON system employing a 10-GHz-based transceiver," Opt. Express **19**(18), 17546–17556 (2011).
3. C. Qin, V. Houtsma, D. Van Veen, J. Lee, H. Chow, and P. Vetter, "40 Gbps PON with 23 dB power budget using 10 Gbps optics and DMT," in *Optical Fiber Communication Conference*, (Optical Society of America, 2017), pp. M3H–5.
4. P. Vetter, D. Suvakovic, H. Chow, P. Anthapadmanabhan, K. Kanonakis, K.-L. Lee, F. Saliou, X. Yin, and B. Lannoo, "Energy-efficiency improvements for optical access," IEEE Commun. Mag. **52**(4), 136–144 (2014).
5. J. von Hoyningen-Huene, C. Ruprecht, A. Ali, and W. Rosenkranz, "Experimental IM/DD OFDMA transmission with scalable receiver frontend for PON scenarios," in *OFC/NFOEC*, (IEEE, 2012), pp. OW4B–6.
6. R. Rosales, I. Cano, D. Nesset, R. Brenot, N. Dubrovina, E. Durán-Valdeiglesias, and H. Debregeas, "Achieving high budget classes in the downstream link of 50G-PON," J. Opt. Commun. Netw. **13**(8), D13–D21 (2021).
7. D. van Veen and V. Houtsma, "Strategies for economical next-generation 50G and 100G passive optical networks," J. Opt. Commun. Netw. **12**(1), A95–A103 (2020).
8. V. Houtsma and D. van Veen, "Optical strategies for economical next generation 50 and 100G PON," in *Optical Fiber Communication Conference*, (Optica Publishing Group, 2019), pp. M2B–1.
9. W. Liang, H. Wang, J. Wei, J. Zhou, D. Guo, and W. Liu, "DSP-enabled 50G OOK-PON with beyond 29 dB power budget using O-band 10G DML and 10G APD," Opt. Commun. **504**, 127486 (2022).
10. P. Torres-Ferrera, H. Wang, V. Ferrero, M. Valvo, and R. Gaudino, "Optimization of band-limited DSP-aided 25 and 50 Gb/s PON using 10G-class DML and APD," J. Lightwave Technol. **38**(3), 608–618 (2020).
11. T. Pfeiffer, P. Dom, S. Bidkar, F. Fredricx, K. Christodoulopoulos, and R. Bonk, "PON going beyond FTTH [Invited Tutorial]," J. Opt. Commun. Netw. **14**(1), A31–A40 (2022).
12. J. S. Wey, D. Nesset, M. Valvo, K. Grobe, H. Roberts, Y. Luo, and J. Smith, "Physical Layer Aspects of NG-PON2 Standards—Part 1: Optical Link Design [Invited]," J. Opt. Commun. Netw. **8**(1), 33–42 (2016).
13. G. Simon, F. Saliou, P. Chanclou, L. A. Neto, and H. H. Elwan, "50Gb/s TDM PON Digital signal processing challenges: mining current G-PON field data to assist higher speed PON," in *2020 European Conference on Optical Communications (ECOC)*, (IEEE, 2020), pp. Tu2J–7.
14. J. Zhou, J. He, X. Lu, G. Wang, Y. Bo, G. Liu, Y. Huang, L. Li, C. Yang, H. Wang, W. Mo, W. Liu, C. Yu, and Z. Li, "100G fine-granularity flexible-rate passive optical networks based on discrete multi-tone with PAPR optimization," J. Opt. Commun. Netw. **14**(11), 944–950 (2022).
15. D. Che, J. Cho, and X. Chen, "Does probabilistic constellation shaping benefit IM-DD systems without optical amplifiers?" J. Lightwave Technol. **39**(15), 4997–5007 (2021).
16. G. Liu, G. Wang, Y. Huang, J. He, Y. Bo, K. Zheng, M. Li, Y. Wu, Y. Lu, Z. Ye, W. Mo, J. Zhou, and L. Li, "World's First Demonstration of Real-time Symmetric Flexible Rate PON with Entropy-Loading and 10G-class Optics," in *European Conference and Exhibition on Optical Communication*, (Optica Publishing Group, 2022), pp. Th3A–3.
17. M. P. Yankov, D. Zibar, K. J. Larsen, L. P. Christensen, and S. Forchhammer, "Constellation shaping for fiber-optic channels with QAM and high spectral efficiency," IEEE Photonics Technol. Lett. **26**(23), 2407–2410 (2014).
18. T. Fehenberger, A. Alvarado, G. Böcherer, and N. Hanik, "On probabilistic shaping of quadrature amplitude modulation for the nonlinear fiber channel," J. Lightwave Technol. **34**(21), 5063–5073 (2016).
19. F. Li, X. Li, J. Yu, and L. Chen, "Optimization of training sequence for DFT-spread DMT signal in optical access network with direct detection utilizing DML," Opt. Express **22**(19), 22962–22967 (2014).
20. M. Yin, Z. Luo, D. Zou, X. Yi, Z. Li, and F. Li, "Demonstration of 100Gb/s/λ 32QAM-DMT Transmission in Intra-DCI Using 10G-calss EML Modulator and 4-bit DAC," in *Asia Communications and Photonics Conference*, (Optical Society of America, 2021), pp. T2H–2.

21. H. Wang, W. Mo, G. Liu, W. Liu, D. Guo, C. Yu, and J. Zhou, "Performance Comparison of OOK, PAM4 and DMT for 50Gb/s Passive Optical Networks," in *2022 IEEE/CIC International Conference on Communications in China (ICCC)*, (IEEE, 2022), pp. 821–825.

22. T. Jiang, W. Xiang, P. C. Richardson, J. Guo, and G. Zhu, "PAPR reduction of OFDM signals using partial transmit sequences with low computational complexity," IEEE Trans. Broadcast. **53**(3), 719–724 (2007).

23. S. Janaaththanan, C. Kasparis, and B. G. Evans, "A gradient based algorithm for PAPR reduction of OFDM using tone reservation technique," in *VTC Spring 2008-IEEE Vehicular Technology Conference*, (IEEE, 2008), pp. 2977–2980.

24. T. Ginige, N. Rajatheva, and K. M. Ahmed, "Dynamic spreading code selection method for PAPR reduction in OFDM-CDMA systems with 4-QAM modulation," IEEE Commun. Lett. **5**(10), 408–410 (2001).

25. S. H. Han and J. H. Lee, "An overview of peak-to-average power ratio reduction techniques for multicarrier transmission," IEEE Wireless Commun. **12**(2), 56–65 (2005).

26. X. Zhu, W. Pan, H. Li, and Y. Tang, "Simplified approach to optimized iterative clipping and filtering for PAPR reduction of OFDM signals," IEEE Trans. Commun. **61**(5), 1891–1901 (2013).

27. R. J. Baxley, C. Zhao, and G. T. Zhou, "Constrained clipping for crest factor reduction in OFDM," IEEE Trans. Broadcast. **52**(4), 570–575 (2006).

28. L. Wang and C. Tellambura, "A simplified clipping and filtering technique for PAR reduction in OFDM systems," IEEE Signal Process. Lett. **12**(6), 453–456 (2005).

29. J. Armstrong, "Peak-to-average power reduction for OFDM by repeated clipping and frequency domain filtering," Electron. Lett. **38**(5), 246 (2002).

30. J. Zhou, L. Li, J. He, X. Lu, Y. Bo, G. Wang, Y. Huang, G. Liu, Y. Lu, S. Gao, Y. Feng, S. Zhao, W. Liu, C. Yu, and Z. Li, "Clipping discrete multi-tone for peak-power-constraint IM/DD optical systems," Sci. China Inf. Sci. (to be published).

31. J. Zhou, J. He, X. Lu, G. Wang, Y. Bo, G. Liu, Y. Huang, L. Li, H. Wang, W. Mo, W. Liu, C. Yu, and Z. Li, "First 100Gb/s Fine-Granularity Flexible-Rate PON Based on Discrete Multi-Tone and PAPR Optimization," in *Optical Fiber Communication Conference*, (Optica Publishing Group, 2022), pp. Th2A–23.

32. J. Zhou, Q. Sui, and Z. Li, "Non-Orthogonal Discrete Multi-Tone: Toward Higher Spectral Efficiency for Optical Networks," IEEE Commun. Mag. **59**(10), 70–75 (2021).

33. D. J. MacKay, "Good error-correcting codes based on very sparse matrices," IEEE Trans. Inf. Theory **45**(2), 399–431 (1999).

34. F. Buchali, F. Steiner, G. Böcherer, L. Schmalen, P. Schulte, and W. Idler, "Rate adaptation and reach increase by probabilistically shaped 64-QAM: An experimental demonstration," J. Lightwave Technol. **34**(7), 1599–1609 (2016).